Published in final edited form as:
Nanomedicine. 2014 April ; 10(3): 491–501. doi:10.1016/j.nano.2013.10.010.

Photoactivated rose bengal functionalized chitosan nanoparticles produce antibacterial/biofilm activity and stabilize dentin-collagen

Annie Shrestha, MSc[a], **Michael R. Hamblin, PhD**[b], and **Anil Kishen, PhD**[a,*]

[a]Discipline of Endodontics, Faculty of Dentistry, University of Toronto, 124 Edward Street, Toronto, ON M5G 1G6, Canada

[b]Wellman Center for Photomedicine, Massachusetts General Hospital, Boston, MA 02114

[b]Department of Dermatology, Harvard Medical School, Boston, MA 02115

[b]Harvard-MIT Division of Health Sciences and Technology, Cambridge, MA 02139

Abstract

Treatment of infected teeth presents two major challenges: persistence of the bacterial-biofilm within root canals after treatment and compromised structural integrity of the dentin hard-tissue. In this study bioactive polymeric chitosan nanoparticles functionalized with rose-bengal, CSRBnp was developed to produce antibiofilm effects as well as stabilize structural-integrity by photocrosslinking dentin-collagen. CSRBnp was less toxic to fibroblasts and had significant antibacterial activity even in the presence of bovine serum albumin. CSRBnp exerted antibacterial mechanism by adhering to bacterial cell surface, permeabilizing the membrane and lysing the cells subsequent to photodynamic treatment. Photoactivated CSRBnp resulted in reduced viability of *Enterococcus faecalis* biofilms and disruption of biofilm structure. Incorporation of CSRBnp and photocrosslinking significantly improved resistance to degradation and mechanical strength of dentin-collagen ($p<0.05$). The functionalized chitosan nanoparticles provided a single-step treatment of infected root dentin by combining the properties of chitosan and that of photosensitizer to eliminate bacterial-biofilms and stabilize dentin-matrix.

Keywords

Functionalized nanoparticles; chitosan; biofilms; collagen; dentin; photodynamic therapy

Introduction

Approximately 60% of human infections are associated with bacterial-biofilms, which include both implant-related infections and chronic non-implant related infections. [1] Likewise the rate of root canal treatment failure of infected teeth has not decreased below 18–26% even with advanced therapeutic options to improve the treatment outcome. [2,3] The widespread recognition of biofilm as the main factor in dental infection has led research towards improved antimicrobial treatment strategies. [4] Another significant issue in

*Corresponding author: Anil Kishen, Discipline of Endodontics, Faculty of Dentistry, University of Toronto, 124 Edward Street, Toronto, ON M5G 1G6, Canada, Phone: 1-4169794900 (4468); Fascimile: 1-4169794936, (anil.kishen@utoronto.ca).

antimicrobial treatments is that the agents need to be selective in eliminating bacteria while sparing the adjacent mammalian cells, which allows targeted antibacterial activity. Targeted antibacterial activity is an advantageous feature in infected hard tissue management. Compromised mechanical integrity and chemical stability due to disease-mediated degradation of the dentin hard tissues caused by host/bacterial proteases [5], and treatment-associated tissue changes have been reported. [6] However, little attention has been paid towards improving the chemical stability and mechanical properties of these previously infected hard tissues. Thus the two major challenges in the management of infected dental hard tissue are (1) decontamination of bacterial-biofilm from the root canals and (2) repair of disease-mediated hard tissue changes. Although approaches that counter these challenges should lead to improved treatment outcomes, currently there is no treatment in dentistry that would produce significant antibiofilm efficacy and at the same time enhance the ultrastructural integrity of dentin tissue in infected teeth.

PDT has been applied in biomedicine owing to its broad-spectrum antimicrobial activity [7] and ability to produce crosslinking of proteins and collagen. [8,9] The singlet oxygen produced facilitates the formation of inter- and intra-molecular covalent cross-links in collagen molecules and other available proteinaceous active sites in the presence of appropriate photosensitizers such as rose bengal (RB). [9] Incorporation and crosslinking of biopolymers such as elastin and chitosan with collagen has been reported to reinforce the collagen scaffolds. [10–12]

Chitosan (CS) is a derivative of chitin, the second most abundant natural biopolymer, and has received significant interest in the fields of biomedicine, food industries, agriculture and environmental science. [13] It shows a broad range of antimicrobial activity, and has biocompatible and biodegradable properties. [14–16] This hydrophilic biopolymer with a large number of free hydroxyl and amino groups has been used for numerous chemical modifications. [12,17] CS polymers have also been considered structurally similar to extracellular matrix components. [18] CS nanoparticles showed marginal reduction of bacterial-biofilm counts following prolonged interaction time. [15]

Functionalized nanoparticles containing various reactive molecules and decorated with peptides or other ligands have led to new possibilities of combating antimicrobial resistance. [19,20] These modified nanomaterials offer unique physicochemical properties, such as ultra-small sizes, large surface area/mass ratio and increased chemical reactivity. Immobilization of photosensitizers on polymeric supports avoided the toxic side effects of residual photosensitizers and provided an added advantage of stability in the physiologic environment. [17,21] Although photosensitizers have been conjugated with different readily available synthetic polymers and liposomes, naturally occurring biopolymers such as CS provide clear advantage of biocompatibility when applied *in vivo*. [17,21] Nanoparticles either encapsulated or surface modified with photosensitizer have been proposed to enhance antimicrobial photodynamic therapy (PDT). [22,23] However, the compromised antibacterial efficacy of PDT in the presence of protein rich media or serum [24,25] needs to be addressed prior to *in vivo* application. The aim of the current work was to synthesize, characterize and assess the antibacterial/antibiofilm efficacy and dentin-collagen stabilization effect of a RB functionalized CS nanoparticles (CSRBnp). CSRBnp is expected to eliminate bacterial biofilms as well as stabilize the dentin-collagen matrix due to the synergistic effect of polycationic bioactive chitosan nanoparticles and singlet oxygen produced by the photosensitizer fraction upon photoactivation.

Methods

All the chemicals used in this study were of analytical grade and were purchased from Sigma-Aldrich (St. Louis, USA) unless noted otherwise.

Synthesis of CSRBnp

CSRBnp was synthesized by conjugating CSnp with RB (Figure 1, *A*). CSnp was synthesized according to the method reported in an earlier work [14] and chemically crosslinked to RB using *N*-ethyl-*N*′-(3-dimethyl aminopropyl) carbodiimide (EDC 5 mM) and N- Hydroxysuccinimide (NHS 5 mM). The CSRBnp formed was dialyzed (Sigma, cellulose tubing, cut off 12000–14000 g/mol) for 1 week, the filtrate was then freeze-dried starting at −80 °C.

Characterization of CSRBnp

Size of the synthesized CSRBnp was determined using transmission electron microscopy (TEM). Absorption spectra for conjugated (CSRBnp) and unconjugated (RB) photosensitizer solutions were recorded using UV-Visible spectroscopy (Epoch, Biotek, USA). Photophysical characterization of CSRBnp to determine the ratio of monomer to dimer (absorbance at 550 nm to 528 nm) at different concentrations was also carried out. [26] The effective concentration of CSRBnp was determined based on the highest monomer:dimer ratio (least aggregation). The conjugated CSRBnp was analyzed for their chemical composition using Fourier Transform Infrared (FTIR) spectrophotometer (Shimadzu, Kyoto, Japan) (16 cm^{-1} resolutions, 32 scans/sample). Photo-oxidative characterization was conducted to assess the ability to generate singlet oxygen by CSRBnp as described previously. [27] A broad-spectrum Lumacare (LumaCare Inc., NewPort Beach, CA, USA) lamp fitted with a 540+/−15 nm filtered fiber (output power= 50 mW) was used as a light source.

Cytotoxicity of CSRBnp

Approximately 10^5 NIH 3T3 mouse fibroblast cells (American Type Culture Collection CCL 1, Rockville, MD) were seeded into 24 well plates in Dulbecco's Modified Eagle medium (DMEM) supplemented with 10% bovine serum and antibiotics and incubated for 48 h in 5% CO_2. After incubation, CSRBnp and RB dissolved in DMEM were added to the cells and incubated for 15 minutes in dark. The cells were irradiated for a total dose of 20 J/cm^2. RB and CSRBnp were also tested without irradiation. Cell survival was determined by the standard 3-(4, 5-dimethylthiazol- 2-yl)-2, 5-diphenyltetrazolium bromide (0.5 mg% MTT) assay that determines the mitochondrial activity. [28] Percentage survival was calculated based on control sample without any treatment as 100%. All analyses were repeated three times in triplicate, and the statistical significance was analyzed by one-way analysis of variance.

Mechanism of antibacterial effect of CSRBnp

Bacterial membrane damage was assessed after treatment with CSRBnp using absorbance at 260 nm and transmission electron microscopy (TEM). Overnight cultures of *Enterococcus faecalis* (ATCC 29212) was washed twice in sterile deionized-water (4000 rpm, 10 minutes, 4 °C) and adjusted to 10^8 CFU/mL (optical density ≈ 0.7) at 600 nm. *E. faecalis* is a Gram-positive, facultative anaerobic bacteria found in high prevalence in persistent infections following root canal treatment. [29] Aliquots of cell suspension (1 mL) were then centrifuged and the cell pellets were treated with different photosensitizer solutions (37 °C for 15 minutes), protected from ambient light. Once the bacterial membrane is compromised, release of cytoplasmic constituents such as DNA and RNA can be monitored through the

detection of absorbance at 260 nm (OD_{260}). [30] The release kinetics of intracellular contents was measured using the absorbance of the bacterial cell filtrate. For PDT, the photosensitized cells were centrifuged and cell pellets irradiated (5 J/cm^2, 540 nm). The % change in OD_{260} at 15 minutes post sensitization and after PDT was calculated with respect to the OD_{260} of the sample measured at 0 minute. The time dependent effect of CSRBnp without light activation was also monitored at different time intervals. All specimens for the TEM were prepared following previous protocol. [6] The bacterial cells were pelleted and fixed in 2.5% glutaraldehyde (0.1 M phosphate buffer) (overnight). The 90 nm thick sections were prepared and examined under TEM (Hitachi H-7000, Tokyo) at 80 kV.

Uptake of CSRBnp by bacterial-biofilm

Uptake of RB and CSRBnp by 7 day old biofilms of *E. faecalis* was evaluated to compare the affinity of anionic RB and cationic CSRBnp. Biofilms were grown in 24 well plates by adding 1 mL of *E. faecalis* culture into each well and incubated at 37 °C, 100 rpm (media was replenished every 48 h). Different concentrations of CSRBnp (0.3, 0.5 & 1 mg/mL) and RB (10, 25, 50 & 100 μM) were added to the biofilm and incubated at 37 °C for 15 minutes, protected from ambient light. Three samples were used for each concentration. Excess CSRBnp and RB were removed leaving behind the bound photosensitizers in biofilm, washed once and the cell-bound photosensitizers extracted using 2% sodium dodecyl sulfate. Quantification of photosensitizer was done spectrophotometrically at the absorption maxima of the RB (550 nm). Uptake values were expressed as the total RB concentration (μM) extracted from biofilm bacteria.

Effect of BSA on the antibacterial efficacy of CSRBnp

RB and CSRBnp were evaluated for the antibacterial efficacy in the presence and absence of 2% bovine serum albumin (BSA). [31] Two concentration of CSRBnp (0.1 and 0.3 mg/mL) was tested with PDT dosage of 2 and 5 J/cm^2. The BSA effect was tested by adding BSA into 1 mL of RB and CSRBnp and incubated at 37°C for 1 h. The photosensitizers with and without BSA were added to the cell pellets of *E. faecalis* (10^8 CFU/ml) and photosensitized for 15 minutes in dark. Following the photosensitization, bacterial cells were centrifuged to remove the unbound photosensitizers and subjected for PDT (5 and 10 J/cm^2). The samples were quantified immediately after PDT and continued incubation for 24 h. Bacterial survival was quantified by plating 50 μL of samples onto freshly poured BHI agar plates.

Assessment of antibacterial/biofilm efficacy of CSRBnp

Monospecies biofilms of *E. faecalis* were grown for 21 days as mentioned above. The biofilm-bacteria was sensitized either with CSRBnp (0.1 & 0.3 mg/mL) or RB (10 μM) for 15 minutes and exposed to PDT with different doses. In case of PDT, the sensitized biofilm bacteria were irradiated using 540 nm fiber, with dosage of 20, 40 and 60 J/cm^2; and fractionated dosage of 10 and 20 J/cm^2 twice. After treatment, biofilm bacteria were disrupted mechanically and quantified using culture method. Colonies were counted after 24 h of incubation at 37 °C and expressed as log CFU/mL. The experiments were carried out in triplicates and the mean values were calculated.

The structure of the biofilms following CSRBnp treatment was assessed using confocal laser scanning microscopy (CLSM) (Olympus IX81 inverted fluorescence microscope SU X1 with spinning disk confocal scan head, Tokyo, Japan). The biofilm-structures were assessed after staining with Live/Dead *Baclight* stain (Molecular Probes, Eugene, OR) in the dark for 10 minutes. Diode-pumped solid state laser lines (Spectral Applied Research,) was the source of illumination with 491 nm excitation and long-pass 525 nm +/−50, and 700 nm +/−75 emission filter settings for green and red signals respectively. Nine different areas were imaged from each sample using a 60x oil immersion objective. The optical sections of the

biofilm-structure were recorded and analyzed using velocity software. Student *t*-test was used to compare the thickness of the biofilm before and after nanoparticles treatment.

Effect of CSRBnp on photodynamic crosslinking of dentin-collagen

Sixteen freshly extracted human incisors and eight bovine incisors were stored in 0.9% saline until use. Bovine teeth were used for mechanical testing (*n = 4*) while human teeth were used for chemical and enzymatic-degradation analysis (*n = 8*). Dentin sections of 12×2×0.5 mm^3 (human) and 16×2×0.2 mm^3 (bovine) were prepared from either side of the root canal lumen. [32] The dentin sections were demineralized in 1M ethylenediaminetetraacetic acid (EDTA, pH = 7.4) for 7 days. The demineralized dentin-collagen specimens (total- 48) were randomly divided into four treatment groups *(n = 12)*: 1) No-treatment - (Control); 2) 2.5% glutaraldehyde (GD) (positive control); 3) RB 10 μM (RB); and 4) CSRBnp 0.3 mg/mL (CSRBnp). The dentin-collagen samples were crosslinked with GD for a period of 6 h. In photodynamic crosslinking, collagen-samples were immersed in 1 mL of RB or CSRBnp solution for 15 minutes and the photosensitized collagen was photoactivated (20 J/cm^2). Crosslinked specimens were thoroughly washed in deionized-water three times and lyophilized for 24 h, for the enzymatic degradation analysis. The bovine dentin-collagen specimens were maintained in deionized-water to be used for mechanical testing.

Enzymatic degradation of the dentin-collagen specimens using collagenase from *Clostridium histolyticum* with an activity of 125 CDU mg^{-1} solid (P/N C-0130; Sigma) was conducted to quantify the amino acid release using a ninhydrin assay as described by Mandl *et al.* [33] at 1, 7 and 14 days. The fully hydrated bovine dentin-collagen specimens from all four test groups were used for tensile testing (Instron 5544, Instron corporation, Canton, MA) with a 100 N load cell, at a crosshead speed of 1 mm/minute until failure occurred. Care was taken to keep the samples hydrated at all times during the test. The ultimate tensile strength and toughness (MPa), were calculated using OriginPro 8.1 software (OriginLab Corporation, MA). Four specimens from each group were fixed in 2.5% glutaraldehyde and processed for TEM evaluation. [6]

Results

Synthesis and characterization of CSRBnp

Figure 1, *B* showed the aggregates of spherical CSRBnp under TEM. The absorption spectra obtained for CSRBnp displayed bands characteristic of RB (Figure 1, *C*). The amount of RB bound in the conjugated CSRBnp was calculated to be 14 μM per 0.1 mg/mL. Based on the absorption spectra the monomer to dimer ratio was calculated for various concentration of CSRBnp. CSRBnp at 0.3 mg/mL concentration showed least aggregation with highest monomer to dimer ratio. FTIR spectra of conjugated CSRBnp showed bands, which could be assigned to the amide bonds between CS and RB (Figure 1, *D*). Two characteristic peaks at 1651 (amide I, carbonyl stretching vibration) and 1558 cm^{-1} corresponding to (NH_2 bending) were prominent in the CS spectra. [17] The ratio of intensities at 1558 and 1652 cm^{-1} was lower in CS as compared to the ratio at 1446 and 1582 cm^{-1} in CSRBnp, which is suggestive of the utilization of free amine groups of CSnp to form bonds with CO- group of RB. The peak (900–1100 cm^{-1}) corresponding to the saccharide group of CS was also prominent in the CSRBnp. The presence of saccharide peak and decreased amide I peak indicated chemical conjugation of RB with CSnp. A shift from 3348 to 3459 cm^{-1}, and a sharper peak in the CSRBnp indicated that the hydrogen bonding was enhanced. The CSRBnp possessed a zeta potential of +30±0.8 mV as a result of the free amine groups from the CSnp. CSRBnp produced singlet oxygen upon photoactivation similar to RB, as observed by the decrease in the DPBF concentration (Figure 1, *E*).

Cytotoxicity of CSRBnp

CSRBnp did not exhibit dark toxicity after 15 min exposure with 95.5±12% cell survival. However, following irradiation cell survival reduced to 72.86±9%. As reported previously, the microparticles of CSRB showed higher toxicity (<50%) after PDT. [34] RB showed significantly higher dark toxicity (55.8±2% cell survival) and further reduction of cell survival (51.23±3%) after PDT.

Mechanism of antibacterial effect of CSRBnp

Following PDT with both RB and CSRBnp bacterial suspensions showed increased absorbance at 260 nm compared to the dark value (Figure 2, *A*). Interaction of CSRBnp and bacteria in the dark resulted in bacterial membrane damage and subsequent leakage of cellular constituents (Figure 2, *B*). With increase in interaction time (2 and 8 h), CSRBnp 0.3 mg/ml showed a higher ability to induce bacterial membrane damage as compared to RB. TEM images further provided information on the bacterial morphology at the ultrastructural level wherein details of membrane integrity and its disruption could be evaluated. Following CSRBnp treatment in the dark for 15 min, the nanoparticles were found to adhere to the bacterial cell walls (Figure 3, *A* and *B*). The well-defined cell borders and dark cytoplasm were observed. Subsequent exposure to PDT resulted in mostly dead bacterial cells. The cell surface was irregular and various stages of cell membrane damage and leakage of cell constituents were evident (Figure 3, *C* and *D*). In case of RB as the photosensitizer, following PDT both dead and viable cells could be found in approximately equal numbers (Figure 3, *E*).

Uptake of CSRBnp by bacterial-biofilm

Bacterial-biofilms showed significantly high uptake of CSRBnp as compared to RB (Table 1).

Effect of BSA on the antibacterial efficacy of CSRBnp

CSRBnp showed excellent antibacterial efficacy with complete bacterial elimination at 2 J/cm^2 (Figure 4, *A*). The dark toxicity of CSRBnp also was significantly higher as compared to RB and increased with increase in the CSRBnp concentration. RB required higher PDT dosage as compared to CSRBnp for complete bacterial elimination. BSA inhibited antibacterial effect of both RB and CSRBnp even after PDT with 10 J/cm^2 (Figure 4, *B*). When the irradiated bacterial cells were incubated for 24 h, CSRBnp produced significant bacterial reduction which was not seen with RB.

Assessment of antibacterial/biofilm efficacy of CSRBnp

CSRBnp demonstrated photodynamic antibacterial efficacy against planktonic (data not shown) and biofilms of *E. faecalis* (Figure 4, *C* and *D*). Both CSRBnp and RB did not show complete killing even after 60 J/cm^2 (Figure 4, *C*). Fractionation of PDT dosage was found to be more effective with complete elimination of biofilm bacteria with CSRBnp (0.3 mg/mL) and in case of RB (Figure 4, *D*). Figure 5 showed the CLSM images of the bacterial-biofilms structure before and after PDT treatment using RB and CSRBnp. The initial thickness of biofilm-structure was found to be 39.2±7.3 μm. The thickness of the biofilms reduced significantly to 23.1±5.57 μm ($p < 0.05$) and 13.1±4.3 μm ($p < 0.05$) after RB and CSRBnp treatment respectively. The distribution of viable bacteria was reduced significantly and the multilayered biofilm architecture was completely disrupted following CSRBnp PDT. In case of RB the mat like biofilm architecture was persistent and few live cell aggregates were still present.

Effect of CSRBnp on photodynamic crosslinking of dentin-collagen

The quantity of amino acids released following enzymatic degradation of the crosslinked and non-crosslinked dentin-collagen was significantly different as a function of time ($p<0.05$) (Table 2). After 14 days the control group specimens disintegrated completely and released the highest amount of amino acid (11.74 μmol/ml). The GD group showed the highest resistance to collagenase degradation even on the 14th day (0.41 μmol/ml). CSRBnp crosslinked dentin-collagen showed slightly faster degradation as compared to RB but was not statistically significant on day 14.

The tensile testing used provided information on the mechanical properties such as UTS and toughness after chemical/photodynamic crosslinking of dentin-collagen specimens [35,36] (Table 3). GD crosslinked dentin-collagen samples showed brittle behavior due to increased UTS and decreased percentage elongation. The samples crosslinked using GD showed reduction in toughness whereas RB and CSRBnp showed significant increase in toughness compared to the control group samples ($p<0.05$). TEM micrographs from the control group revealed a collagen matrix that contained intact, banded collagen fibrils (Figure 6, *A*). Treatment with collagenase, resulted in the degradation and loss of normal fibrillar pattern in collagen (Figure 6, *B*). Following crosslinking using CSRBnp, the arrangements of the collagen fibrils were denser with smooth edges (Figure 6, *C*). The surface of the crosslinked collagen showed a layer of collagen fibrils and CSRBnp incorporated within the collagen mesh and could be seen as aggregates on the surface (White arrows) (Figure 6, *D*). The CSRBnp crosslinked dentin-collagen showed resistance to enzymatic degradation (Figure 6, *E* and *F*).

Discussion

The primary focus of this study was to further improve the antibacterial/antibiofilm efficacy of PDT as well as stabilize dentin-collagen by synthesizing a CS nanoparticles functionalized with photosensitizer (CSRBnp). CSRBnp showed characteristics of both the bioactive polymer and photosensitizer as determined by the absorption and FTIR spectra and released singlet oxygen upon photoactivation. The binding of RB to the polymeric CSnp as well as oxygen scavenging ability [37] of CS could have contributed to the reduced rate of singlet oxygen yield. This slower release of singlet oxygen as observed with CSRBnp could provide sufficient time for molecular oxygen to be replenished at the site of PDT and prolong the antibacterial effect. [22] Replenishment of molecular oxygen during this lag phase as shown during fractionation of light dosage [38] could provide possible explanation to the enhanced PDT mediated antibacterial/biofilm effect. The findings from the current experiments, confirmed that conjugating RB with CS nanoparticles abrogated the toxicity towards fibroblasts, as CS has long been known to be highly biocompatible. [39]

Damage to bacterial membrane, increased membrane permeability and subsequent intracellular leakage are the suggested antibacterial effects of CS. [16] The damage to bacterial membrane and leakage of cell constituents with CSRBnp treatment for prolonged time and following PDT was found to be the highest. Cationic micelles when interacting with bacteria have shown similar membrane lysis and release of cell constituents, which has been mainly attributed to the electrostatic interaction and steric hindrance imposed by the micelles surrounding the cells. [40] The increased uptake of CSRBnp into bacterial cells and biofilm structure is mainly attributed to their positive charge and nano-size, which led to not only a greater interaction with bacterial cell but also with the negatively charged polymeric matrix of biofilm. Since the cationic CS nanoparticles and CSRBnp are highly reactive, it may interact physico-chemically with other charged particles in the solution. The tissues and particles present in the vicinity could also act as a potential substrate for highly reactive singlet oxygen. [41] Other than direct inhibition of these nanoparticles, presence of tissue fluid

or BSA is known to reduce the efficacy of antibacterial PDT due to crosslinking action or the compromised half-life of singlet oxygen. [25] The photoactivated CSRBnp showed the best results to eliminate bacteria even in the presence of BSA.

Conjugation of photosensitizer with a cationic molecule allowed photosensitizer molecules to enter the bacterial cells and resulted in increased killing efficiency at lower concentration than neutral and anionic photosensitizer molecules. [42] Similarly, in this study cationic CSRBnp bound to the negatively charged bacterial surface and diffused through the extracellular polymeric substance, thereby facilitating the penetration of the photosensitizer molecule through bacterial membrane and biofilm structure. [43] CSRBnp combined with PDT showed complete elimination of the biofilm structure. Singlet oxygen is known to diffuse approximately 50 nm [44], and the closer proximity of the photosensitizer molecule to the cell surface might have allowed the diffusion of singlet oxygen into the resident bacterial cells. Irradiation for prolonged time periods would deplete the molecular oxygen available in the immediate surrounding of the cells. [38] The slower release of singlet oxygen by CSRBnp as reported in this study and oxygenation of biofilm during fractionation resulted in the complete elimination of biofilm.

Chemical crosslinking requires longer treatment time to establish stable collagen cross-links as compared to the photodynamic process. [10,45] This is a major limitation especially for clinical applications, where shorter treatment time is highly desirable. Photodynamic crosslinking is a rapid process that occurs via the production of singlet oxygen or radicals by the light excited photosensitizers. The photo-oxidized amino acids react with normal or photo-altered residues in another protein molecule resulting in a cross-link. [46]

Bacterial collagenase degrades collagen by hydrolyzing the peptide bond at the amino-terminal of glycine (–X-Gly-Pro). [47] Following crosslinking of collagen, the sites of collagenase attack may be protected or modified, and this may contribute to the significant difference in the release of amino acid residues following enzymatic degradation. [48] In this study, crosslinked collagen showed significantly higher resistance to degradation. Photoactivation of CSRBnp resulted in crosslinking of dentin-collagen and incorporation of CS nanoparticles within the collagen architecture. This resulted in the improved mechanical properties (UTS and toughness). The CS nanoparticles in the collagen matrix may have reinforced the collagen structure by increasing the number of amine reaction sites resulting in the formation of ionic complexes between CS and collagen during crosslinking (refer to graphical abstract). [49]

CSRBnp synthesized and characterized in this study possessed the following beneficial characteristics: (1) CS as an effective broad spectrum antibacterial with biocompatibility; (2) RB as a photosensitizer with photodynamic antibacterial and crosslinking ability; (3) the nano-size further enhanced the photoactive and antimicrobial properties due to high surface area to mass ratio resulting in increased interaction with the substrate (Graphical abstract). Nanoparticles in general possess stability limitations that restrict application *in vivo*. [50] Due to their strong self-reactivity they form aggregates or flocculates thus compromising the available reactive surface area. Furthermore, the root canal system presents a complex anatomical challenge for effective delivery of antimicrobial agents. Efforts to disinfect complex root canal niches that are not accessible to mechanical instruments or liquid chemicals are continuously being investigated. The stability and delivery of these antibacterial nanoparticles into infected dentin tissue needs to be addressed and this is a separate avenue for biophysical research.

As hypothesized, the CSRBnp displayed properties of both CS and RB in a photoactivable nano-structure that performed the dual function of targeted elimination of bacterial-biofilms

and improved mechanical and chemical stability of dentin organic matrix. The present study provides a novel nanoparticle based approach to enhance biofilm elimination and simultaneously restore the ultrastructural integrity of infected dentin tissue, both of which hold equally pivotal status for the long-term treatment success of infected teeth.

Acknowledgments

This work is funded by the University of Toronto and CIHR Training Fellowship (TGF-53877). MRH was funded by the US NIH (R01AI50875).

References

1. Lewis K. Riddle of biofilm resistance. Antimicrob Agents Chemother. 2001; 45:999–1007. [PubMed: 11257008]
2. Gilbert GH, Tilashalski KR, Litaker MS, McNeal SF, Boykin MJ, Kessler AW. Outcomes of root canal treatment in Dental Practice-Based Research Network practices. Gen Dent. 2010; 58:28–36. [PubMed: 20129890]
3. Lumley PJ, Lucarotti PS, Burke FJ. Ten-year outcome of root fillings in the General Dental Services in England and Wales. Int Endod J. 2008; 41:577–85. [PubMed: 18479376]
4. Nair PN. Pathogenesis of apical periodontitis and the causes of endodontic failures. Crit Rev Oral Biol Med. 2004; 15:348–81. [PubMed: 15574679]
5. Vier FV, Figueiredo JA. Internal apical resorption and its correlation with the type of apical lesion. Int Endod J. 2004; 37:730–7. [PubMed: 15479255]
6. Ferrari M, Mason PN, Goracci C, Pashley DH, Tay FR. Collagen degradation in endodontically treated teeth after clinical function. J Dent Res. 2004; 83:414–9. [PubMed: 15111635]
7. Hamblin MR, Hasan T. Photodynamic therapy: a new antimicrobial approach to infectious disease? Photochem Photobiol Sci. 2004; 3:436–50. [PubMed: 15122361]
8. Spikes JD, Shen HR, Kopeckova P, Kopecek J. Photodynamic crosslinking of proteins. III. Kinetics of the FMN- and rose bengal-sensitized photooxidation and intermolecular crosslinking of model tyrosine-containing N-(2-hydroxypropyl)methacrylamide copolymers. Photochem Photobiol. 1999; 70:130–7. [PubMed: 10461454]
9. Chan BP, Chan OC, So KF. Effects of photochemical crosslinking on the microstructure of collagen and a feasibility study on controlled protein release. Acta Biomater. 2008; 4:1627–36. [PubMed: 18640085]
10. Everaerts F, Gillissen M, Torrianni M, Zilla P, Human P, Hendriks M, et al. Reduction of calcification of carbodiimide-processed heart valve tissue by prior blocking of amine groups with monoaldehydes. J Heart Valve Dis. 2006; 15:269–77. [PubMed: 16607911]
11. Madhavan K, Belchenko D, Motta A, Tan W. Evaluation of composition and crosslinking effects on collagen-based composite constructs. Acta Biomater. 2010; 6:1413–22. [PubMed: 19815100]
12. Wang XH, Li DP, Wang WJ, Feng QL, Cui FZ, Xu YX, et al. Crosslinked collagen/chitosan matrix for artificial livers. Biomaterials. 2003; 24:3213–20. [PubMed: 12763448]
13. Yilmaz E. Chitosan: a versatile biomaterial. Adv Exp Med Biol. 2004; 553:59–68. [PubMed: 15503447]
14. Kishen A, Shi Z, Shrestha A, Neoh KG. An investigation on the antibacterial and antibiofilm efficacy of cationic nanoparticulates for root canal disinfection. J Endod. 2008; 34:1515–20. [PubMed: 19026885]
15. Shrestha A, Shi Z, Neoh KG, Kishen A. Nanoparticulates for antibiofilm treatment and effect of aging on its antibacterial activity. J Endod. 2010; 36:1030–5. [PubMed: 20478460]
16. Rabea EI, Badawy ME, Stevens CV, Smagghe G, Steurbaut W. Chitosan as antimicrobial agent: applications and mode of action. Biomacromolecules. 2003; 4:1457–65. [PubMed: 14606868]
17. Moczek L, Nowakowska M. Novel water-soluble photosensitizers from chitosan. Biomacromolecules. 2007; 8:433–8. [PubMed: 17291066]
18. Tan W, Krishnaraj R, Desai TA. Evaluation of nanostructured composite collagen--chitosan matrices for tissue engineering. Tissue Eng. 2001; 7:203–10. [PubMed: 11304455]

19. Veerapandian M, Yun K. Functionalization of biomolecules on nanoparticles: specialized for antibacterial applications. Appl Microbiol Biotechnol. 2011; 90:1655–67. [PubMed: 21523475]
20. Liu L, Xu K, Wang H, Tan PK, Fan W, Venkatraman SS, et al. Self-assembled cationic peptide nanoparticles as an efficient antimicrobial agent. Nat Nanotechnol. 2009; 4:457–63. [PubMed: 19581900]
21. Bonnett R, Krysteva MA, Lalov IG, Artarsky SV. Water disinfection using photosensitizers immobilized on chitosan. Water Res. 2006; 40:1269–75. [PubMed: 16499945]
22. Guo Y, Rogelj S, Zhang P. Rose Bengal-decorated silica nanoparticles as photosensitizers for inactivation of gram-positive bacteria. Nanotechnology. 2010; 21:065102. [PubMed: 20061596]
23. Perni S, Prokopovich P, Pratten J, Parkin IP, Wilson M. Nanoparticles: their potential use in antibacterial photodynamic therapy. Photochem Photobiol Sci. 2011; 10:712–20. [PubMed: 21380441]
24. Dai T, Huang YY, Hamblin MR. Photodynamic therapy for localized infections--state of the art. Photodiagnosis Photodyn Ther. 2009; 6:170–88. [PubMed: 19932449]
25. Bhatti M, MacRobert A, Meghji S, Henderson B, Wilson M. Effect of dosimetric and physiological factors on the lethal photosensitization of Porphyromonas gingivalis in vitro. Photochem Photobiol. 1997; 65:1026–31. [PubMed: 9188283]
26. George S, Kishen A. Photophysical, photochemical, and photobiological characterization of methylene blue formulations for light-activated root canal disinfection. J Biomed Opt. 2007; 12:034029. [PubMed: 17614737]
27. Hadjur C, Lange N, Rebstein J, Monnier P, van den Bergh H, Wagnire G. Spectroscopic studies of photobleaching and photo-product formation of meta(tetrahydroxyphenyl) chlorin(m-THPC) used in photodynamictherapy. The production of singlet oxygen by m-THPC. J Photochem Photobiol B. 1998; 45:170–8.
28. Mosmann T. Rapid colorimetric assay for cellular growth and survival: application to proliferation and cytotoxicity assays. J Immunol Methods. 1983; 65:55–63. [PubMed: 6606682]
29. Hancock HH 3rd, Sigurdsson A, Trope M, Moiseiwitsch J. Bacteria isolated after unsuccessful endodontic treatment in a North American population. Oral Surg Oral Med Oral Pathol Oral Radiol Endod. 2001; 91:579–86. [PubMed: 11346739]
30. Chen CZS, Cooper SL. Interactions between dendrimer biocides and bacterial membranes. Biomaterials. 2002; 23:3359–3368. [PubMed: 12099278]
31. Portenier I, Haapasalo H, Rye A, Waltimo T, Orstavik D, Haapasalo M. Inactivation of root canal medicaments by dentine, hydroxylapatite and bovine serum albumin. Int Endod J. 2001; 34:184–8. [PubMed: 12193263]
32. Carrilho MR, Geraldeli S, Tay F, de Goes MF, Carvalho RM, Tjaderhane L, et al. In vivo preservation of the hybrid layer by chlorhexidine. J Dent Res. 2007; 86:529–33. [PubMed: 17525352]
33. Mandl I, Maclennan JD, Howes EL. Isolation and characterization of proteinase and collagenase from Cl. histolyticum. J Clin Invest. 1953; 32:1323–9. [PubMed: 13109000]
34. Shrestha A, Hamblin MR, Kishen A. Characterization of a conjugate between Rose Bengal and chitosan for targeted antibiofilm and tissue stabilization effects as a potential treatment of infected dentin. Antimicrob Agents Chemother. 2012; 56:4876–84. [PubMed: 22777042]
35. Bedran-Russo AK, Pashley DH, Agee K, Drummond JL, Miescke KJ. Changes in stiffness of demineralized dentin following application of collagen crosslinkers. J Biomed Mater Res B Appl Biomater. 2008; 86B:330–4. [PubMed: 18161815]
36. Wollensak G, Iomdina E. Long-term biomechanical properties of rabbit cornea after photodynamic collagen crosslinking. Acta Ophthalmol. 2009; 87:48–51. [PubMed: 18547280]
37. Tomida H, Fujii T, Furutani N, Michihara A, Yasufuku T, Akasaki K, et al. Antioxidant properties of some different molecular weight chitosans. Carbohydr Res. 2009; 344:1690–6. [PubMed: 19559405]
38. van Geel IP, Oppelaar H, Marijnissen JP, Stewart FA. Influence of fractionation and fluence rate in photodynamic therapy with Photofrin or mTHPC. Radiat Res. 1996; 145:602–9. [PubMed: 8619026]

39. Kumar MN, Muzzarelli RA, Muzzarelli C, Sashiwa H, Domb AJ. Chitosan chemistry and pharmaceutical perspectives. Chem Rev. 2004; 104:6017–84. [PubMed: 15584695]
40. Nederberg F, Zhang Y, Tan JP, Xu K, Wang H, Yang C, et al. Biodegradable nanostructures with selective lysis of microbial membranes. Nat Chem. 2011; 3:409–14. [PubMed: 21505501]
41. Wilson M, Sarkar S, Bulman JS. Effect of Blood on Lethal Photosensitization of Bacteria in Subgingival Plaque from Patients with Chronic Periodontitis. Laser Med Sci. 1993; 8:297–303.
42. Demidova TN, Hamblin MR. Effect of cell-photosensitizer binding and cell density on microbial photoinactivation. Antimicrob Agents Chemother. 2005; 49:2329–35. [PubMed: 15917529]
43. Merchat M, Spikes JD, Bertoloni G, Jori G. Studies on the mechanism of bacteria photosensitization by meso-substituted cationic porphyrins. J Photochem Photobiol B. 1996; 35:149–57. [PubMed: 8933721]
44. Ochsner M. Photophysical and photobiological processes in the photodynamic therapy of tumours. J Photochem Photobiol B. 1997; 39:1–18. [PubMed: 9210318]
45. Rafat M, Li F, Fagerholm P, Lagali NS, Watsky MA, Munger R, et al. PEG-stabilized carbodiimide crosslinked collagen-chitosan hydrogels for corneal tissue engineering. Biomaterials. 2008; 29:3960–72. [PubMed: 18639928]
46. Verweij H, Dubbelman TM, Van Steveninck J. Photodynamic protein cross-linking. Biochim Biophys Acta. 1981; 647:87–94. [PubMed: 7295723]
47. Watanabe K. Collagenolytic proteases from bacteria. Appl Microbiol Biotechnol. 2004; 63:520–6. [PubMed: 14556041]
48. Jayakrishnan A, Jameela SR. Glutaraldehyde as a fixative in bioprostheses and drug delivery matrices. Biomaterials. 1996; 17:471–84. [PubMed: 8991478]
49. Sionkowska A, Wisniewski M, Skopinska J, Kennedy CJ, Wess TJ. Molecular interactions in collagen and chitosan blends. Biomaterials. 2004; 25:795–801. [PubMed: 14609668]
50. Ruenraroengsak P, Cook JM, Florence AT. Nanosystem drug targeting: Facing up to complex realities. J Control Release. 2010; 141:265–76. [PubMed: 19895862]

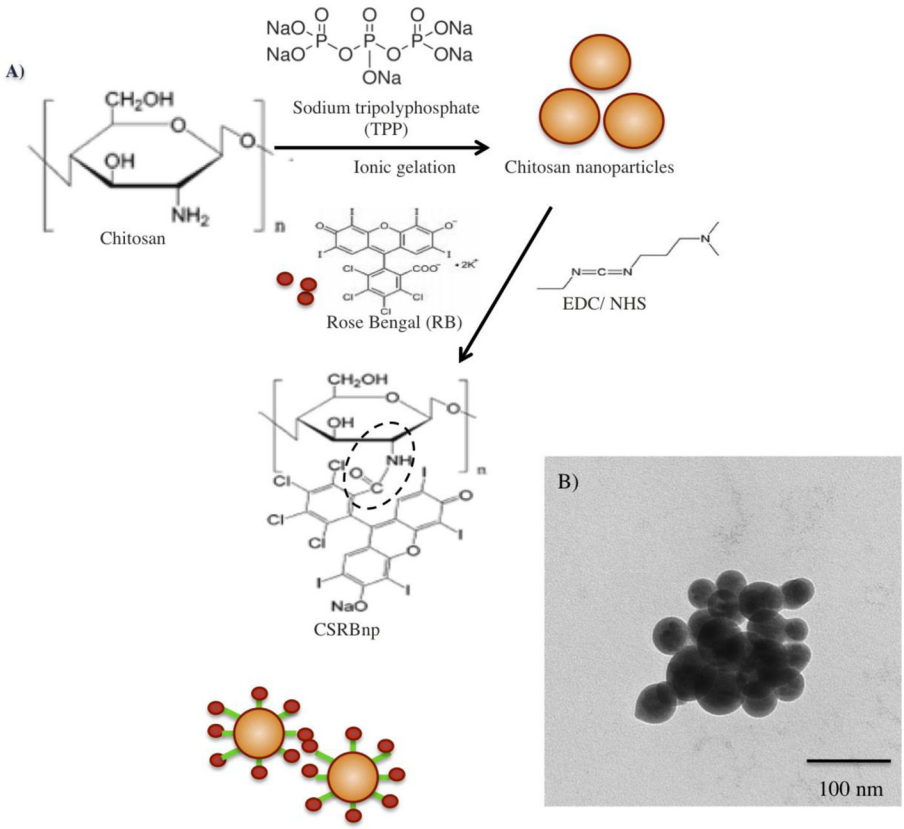

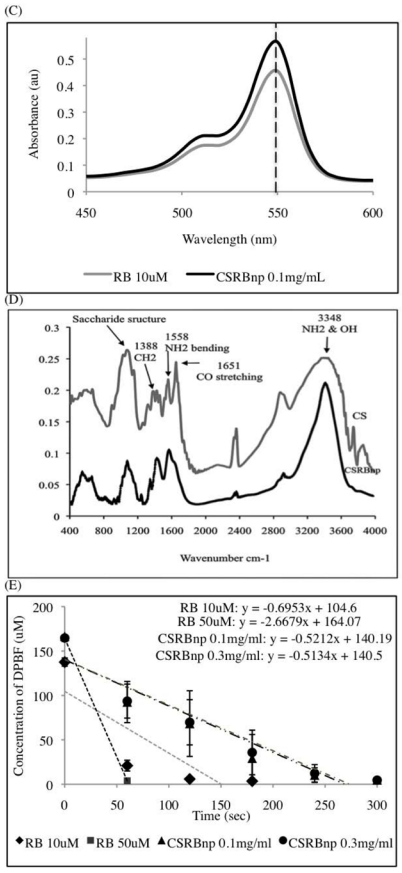

Figure 1.

Chemical reaction during conjugation of CS nanoparticles with rose bengal (RB) in the presence of EDC (*N*-ethyl-*N*′-(3-dimethyl aminopropyl) carbodiimide) and NHS (*N*-Hydroxysuccinimide) **(A)**. Transmission electron microscopy (TEM) image of CSRBnp (scale bar= 100nm). The CSRBnp were of 60±20 nm in size **(B)**. Absorption spectra of RB and CSRBnp with peak maxima at 550 nm **(C)**. FTIR spectra of chitosan and CSRBnp (400 to 4000 cm^{-1} wave number) **(D)**. The singlet oxygen yield monitored photometrically using oxidation of 1,3-diphenylisobenzofuran (DPBF). The rate of singlet oxygen yield in case of CSRBnp was slower than that of RB **(E)**.

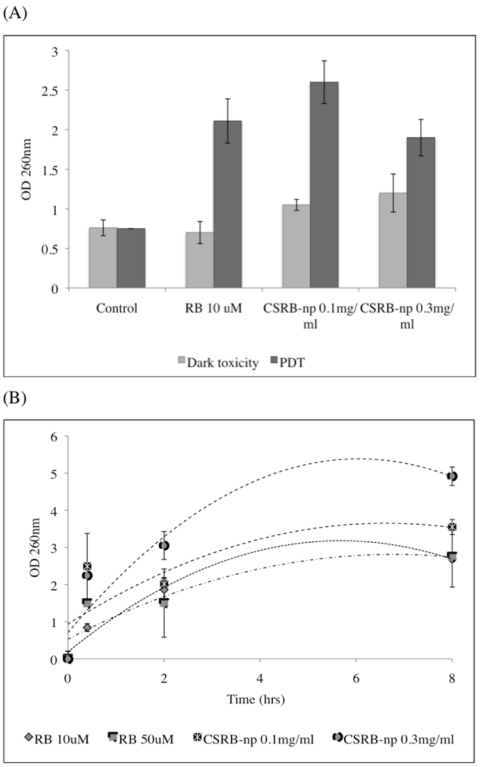

Figure 2.

Graph showing release of cell constituents (absorbance at 260 nm) following treatment with RB and CSRBnp with and without PDT **(A)**. Time dependent release of cell constituents following treatment with RB and CSRBnp **(B)**. With increase in interaction time, CSRBnp showed highest cell membrane damage.

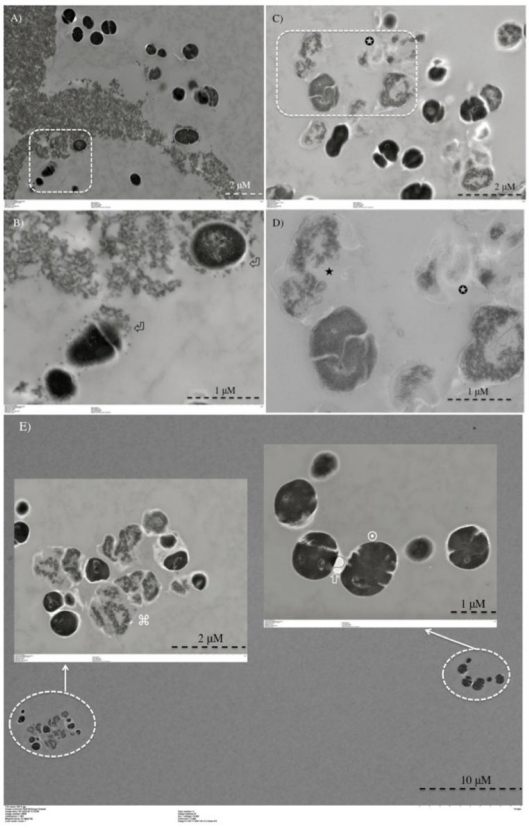

Figure 3.

Transmission electron microscopy images for planktonic *E. faecalis* after treatment with CSRBnp for 15 min (**A and B**). Aggregates of CSRBnp could be seen surrounding the bacterial cell. Nanoparticles were found attached to the bacterial cell surface and forming an envelope (⇦) (**B**). The cells did not show any disruption of morphology. Following PDT of the sensitized bacteria, various stages of membrane damage as well as release of cell constituents were evident (**C and D**). Most of the bacteria showed some kind of cell membrane disruption (□), and release of cell constituents (✉) at higher magnification (**D**). However, the bacterial cells after PDT with RB as the photosensitizer showed both live (¤) and dead (⌘) cells (**E**).

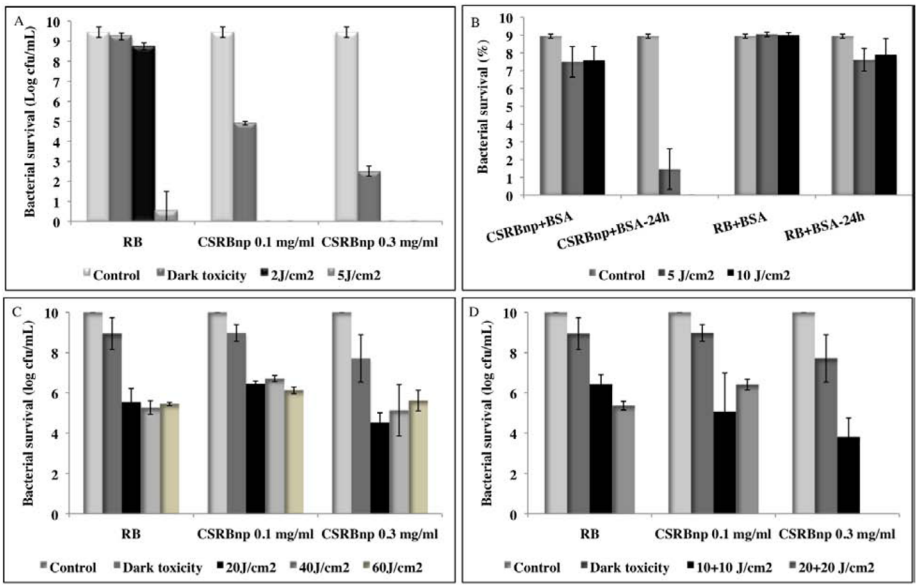

Figure 4.

Bacterial survival of planktonic *E. faecalis* after PDT using RB and CSRBnp (**A**). Bacterial survival of planktonic *E. faecalis* in the presence of bovine serum albumin (BSA) after treatment with different nanoparticles with and without PDT (**B**). CSRBnp after PDT and incubation for 24 hrs showed the best results as compared to CSRBnp and RB with/without PDT. Antibiofilm effect of CSRBnp and RB on 21 days old *E. faecalis* biofilm (**C and D)**. Complete elimination was obtained only after fractionation of PDT dose in case of CSRBnp at the higher concentration (**D**) in contrast to both the photosensitizers even after PDT dosage of 60 J/cm^2 (**C**). Error bars show the standard deviation from average value.

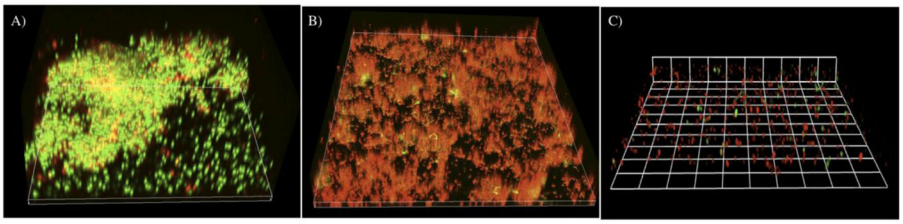

Figure 5.

The three-dimensional confocal laser scanning microscopy reconstruction of the biofilms subjected to PDT using RB and CSRBnp. (**A**) The biofilm receiving no treatment showed a multilayered three dimensional structure with both live (green) and dead (red) cells. (**B**) The biofilms subjected to sensitization with RB and PDT (40J/cm^2) showed significantly higher number of dead cells. The mat like biofilm structure was not disturbed. (**C**) In case of CSRBnp the biofilm structure was completely disrupted with only few live and dead cells remaining on the substrate.

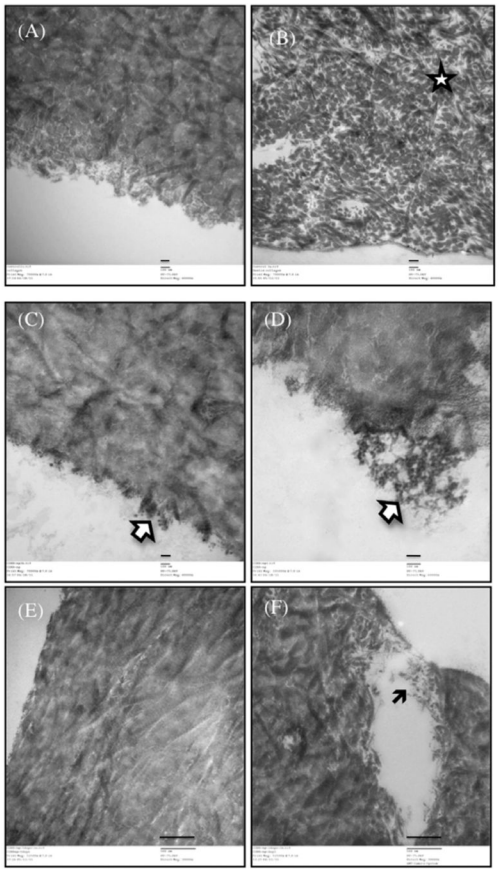

Figure 6.
Transmission electron micrographs of dentin-collagen without any treatment (**A and B**) and following photocrosslinking treatment with CSRBnp (**C–F**). The scale bars in A–D represent 100 nm and in E–F are of 500 nm.

Table 1

Uptake by biofilm bacterial cells obtained after incubation with different photosensitizers.

Photosensitizer	Photosensitizer (μM) uptake mL^{-1} of *E. faecalis* cells
RB 10 μM	2.72±0.15
RB 25 μM	2.80±0.09
RB 50 μM	3.01±0.11
RB 100 μM	3.68±0.17
CSRBnp 0.3 mg mL^{-1}	16.15±5.82
CSRBnp 0.5 mg mL^{-1}	24.06±9.77
CSRBnp 1.0 mg mL^{-1}	40.68±4.32

Values represent the uptake in μM mL^{-1} of cells obtained after incubation of biofilm bacteria with RB and CSRBnp. Values are the means of three readings ± standard deviations. There was a significant increase in uptake of photosensitizer by bacterial cells when conjugated with CS ($P<0.05$).

Table 2

The enzymatic degradation of dentin-collagen with time following different crosslinking procedures. The values represent the amount of amino acid released (μmol ml^{-1}) following degradation of dentin-collagen determined using Ninhydrin assay.

	Day 1	Day 7	Day 14
Control	0.660 (0.71)	9.81 (2.17)	11.74 (1.34)
GD	0.034 [b] (0.012)	0.32 [d] (0.003)	0.41 [f] (0.003)
RB	0.06 [b] 0.02	0.48 [d] (0.31)	1.58 [f] (0.71)
CSRBnp	0.027 [b] (0.003)	1.59 [d] (0.32)	2.51 [f] (0.47)

The results are averaged values obtained with standard deviations in the parentheses. For each column, groups identified by different Roman letters are significantly different ($P < 0.05$).

Table 3

The ultimate tensile strength (UTS) and toughness of dentin collagen following different crosslinking procedures.

	Control	GD	RB	CSRBnp
UTS [MPa]	4.11 [a] (0.78)	8.20 [b] (1.66)	4.14 [a] (0.70)	8.13 [b] (1.76)
Toughness [MPa]	17.49 [c] (0.64)	10.74 [d] (2.66)	51.95 [d] (1.52)	74.31[d] (14.58)

The results are averaged values obtained with standard deviations in the parentheses. For each row, groups identified by different Roman letters are significantly different ($P < 0.05$).